First-principles calculations of the geometry and electronic structure of electron- and hole-doped C_{60} in the field-effect transistor structure

Tadahiko Chida, Shugo Suzuki, and Kenji Nakao
Institute of Materials Science, University of Tsukuba, Tsukuba 305-8573, Japan
(Received 10 April 2003; revised manuscript received 5 December 2003; published 11 May 2004)

We investigate the geometry and electronic structure of field-effect-doped C_{60} by carrying out first-principles calculations based on the density-functional theory. To reproduce field-effect doping, we employ a structural model which consists of a single C_{60} (111) layer and an electrode layer. In this model, we assume that the carrier concentration is higher than one electron or hole per unit cell. We find that the charge distribution on the electrode side hemisphere of the C_{60} molecule, say the north hemisphere, is changed by field-effect doping while that on the south hemisphere is hardly changed. In particular, on the hexagonal face nearest to the electrode, the π-like electron density is considerably increased and decreased in electron- and hole-doped C_{60}, respectively. Therefore, the C-C bonds on this face are elongated with increasing the carrier concentration both in electron- and hole-doped C_{60}. Furthermore, it is found that the potential energy induced by field-effect doping is large enough to change the band dispersion and the density of states. In addition, we discuss the charge distribution at lower carrier concentrations with two models; one is the model consisting of three C_{60} layers and the other is the continuum model.

DOI: 10.1103/PhysRevB.69.205102 PACS number(s): 71.20.Tx, 71.15.−m, 73.20.−r

I. INTRODUCTION

Since the discovery of superconductivity in K_3C_{60},[1] electron- and hole-doped C_{60} has attracted much experimental and theoretical interest. In particular, a variety of electron-doped C_{60} superconductors have been synthesized and it has been established that the transition temperature is increased by expanding the lattice constant, which results in the increase of the density of states at the Fermi level. The highest transition temperature of those compounds is 33 K for $RbCs_2C_{60}$.[2] To obtain compounds with a larger lattice constant, the neutral NH_3 molecule is inserted into K_3C_{60}. However, since the lattice of the synthesized compound, $NH_3K_3C_{60}$, changes from the fcc structure, the superconductivity disappears.[3] One might believe to observe the superconductivity at higher temperatures in hole-doped C_{60} than in electron-doped C_{60} because the density of states of the valence bands of the C_{60} solid is larger than that of the conduction bands. Although halogen doping is one of the candidates to introduce holes into the valence bands, the significant charge transfer between C_{60} and halogen atoms is not observed.[4] Moreover, $(AsF_6)_2C_{60}$ and $(SbF_6)_2C_{60}$ have been synthesized for the purpose of introducing holes.[5] However, metallic and superconducting properties have not been found due to the disorder induced by the intercalation of molecules. As mentioned above, it seems that the intercalation of atoms and molecules has difficulties for the extensive study of electron- and hole-doped C_{60}. Therefore, it is hoped to develop a new method to provide carriers into the C_{60} solid.

The new method using the field-effect transistor (FET) structure, that is, field-effect doping, has recently received much attention as a method to obtain the electron- and hole-doped C_{60} without the disorder. The used FET structure consists of a gate electrode and dielectric and C_{60} layers. In addition, both source and drain are attached to the interface between the dielectric and C_{60} layers to probe the transport properties. Since carriers are injected into C_{60} only by applying a gate voltage, the intercalation of atoms and molecules is not required. In the C_{60} FETs fabricated so far,[6] the carrier concentration has been low. However, if high-quality dielectric and C_{60} layers are prepared, higher gate voltages are achieved and it is possible to vary the sign and concentration of charge carriers over a wide range.

Although field-effect doping is a promising method, the electronic structures realized by this method are not clarified. In FET structures, when applying a gate voltage, the macroscopic electric field is generated and also carriers injected into C_{60} are strongly confined near the surface adjacent to the dielectric layer. In other words, the electrostatic potential and the charge distribution are modulated due to field-effect doping. Thus, it is expected that the electronic structure of field-effect-doped C_{60} is considerably different from those of neutral and alkali-metal-doped C_{60}.

In this paper, we study the geometry and electronic structure of field-effect-doped C_{60} by carrying out first-principles calculations based on the density-functional theory. In Sec. II, we first explain the method of calculations and a used structural model. Next, our results and discussion are given in Sec. III. Finally, we summarize our results in Sec. IV.

II. METHOD OF CALCULATIONS

In the present study, we employ the full-potential linear-combination-of-atomic-orbitals method[7] based on the density-functional theory with the local-density approximation.[8,9] Also, the exchange-correlation potential expressed by the Perdew-Zunger parametrization of Ceperley and Alder is used.[10,11] The number of k points in the full Brillouin zone is six for geometry optimizations and self-consistent calculations. Moreover, we use 441 k points for the calculations of the density of states.

We next explain the basis set used in this study. We use

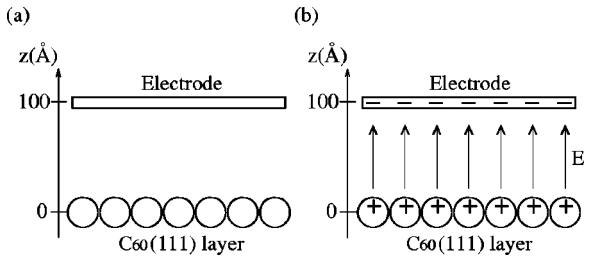

FIG. 1. (a) Schematic diagram of the model for field-effect-doped C_{60}. (b) Situation of hole doping in the model (a). The C_{60} layer is positively charged while the electrode is negatively charged. The uniform electric field is generated between the electrode and C_{60} layers.

$1s$, $2s$, and $2p$ atomic orbitals of neutral carbon atom. Furthermore, we use $2s$ and $2p$ atomic orbitals of $2+$ carbon ion taking into account the effect that atomic orbitals shrink in solids. Also, we use $3d$ atomic orbital $4+$ of carbon ion taking into account the effect of the polarization of electron density.

We also explain our structural model for field-effect-doped C_{60}. In the real C_{60} FET structure, carriers injected into C_{60} may concentrate on the surface adjacent to the dielectric layer because the carriers are attracted by opposite charges on the gate electrode. In other words, the carriers are induced on the surface by the electric field generated by the electrode. To take account of this, we use a structural model which consists of a single C_{60} layer and an electrode layer as shown in Fig. 1(a). We here assume that the single C_{60} layer is the (111) surface layer of the fcc C_{60} solid, whose lattice constant is 14.2 Å. This layer is the two-dimensional triangular lattice whose lattice constant is 10.0 Å and also the unit cell contains one C_{60} molecule. Moreover, we place an electrode layer at $z=100$ Å in parallel to the C_{60} layer at $z=0$ Å. This electrode layer is essential for reproducing field-effect doping. Since the wave functions derived from the electrode do not interfere with the C_{60} layer, we can use artificial electrodes so long as calculations converge. Therefore, the electrode layer used in the present study has the same lattice structure as the C_{60} (111) layer and also the unit cell contains one light atom. Accordingly, the two-dimensional unit cell of our model consists of one C_{60} molecule and one electrode atom.

The calculations for field-effect-doped C_{60} are performed as follows. For instance, we show hole-doped C_{60} in Fig. 1(b). To obtain the desired hole concentration in the C_{60} layer, we remove electrons from the C_{60} layer and place them on the electrode layer. Thus, the C_{60} layer is positively charged while the electrode is negatively charged as shown in Fig. 1(b). This circumstance is corresponding to a charged planar capacitance. Also, when calculating electron-doped C_{60}, we remove electrons from the electrode layer and place them on the C_{60} layer, so that the C_{60} layer is negatively charged while the electrode is positively charged. This circumstance is obtained by changing the sigh of charges in Fig. 1(b). Furthermore, we artificially maintain the desired occupations both in the C_{60} layer and the electrode layer during self-consistent calculations. As a result, the Fermi levels in the two layers are different and the uniform electric field is generated between them. The strength of this electric field is estimated to be $209\times|Q|$MV/cm$(2.09\times|Q|$V/Å$)$, where Q denotes the carrier concentration and its unit is e per unit cell. In this paper, the negative and positive Q mean the electron and hole concentrations, respectively. Since the electrode and C_{60} layers are adequately separated, the transfer and overlap integrals do not exist between them. Consequently, wave functions derived from the electrode do not interfere with the electronic structures of the C_{60} layer. However, the uniform electric field generated by the electrode strongly affects the electronic structures of the C_{60} layer.

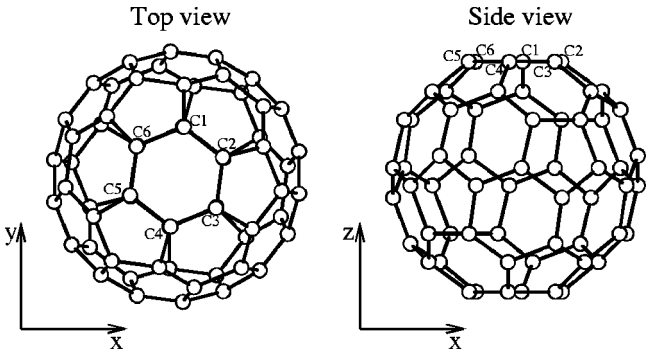

FIG. 2. Orientation of the C_{60} molecule in the unit cell. The z axis is parallel to the threefold axis. The x and y axes are in the (111) plane.

The orientation of the C_{60} molecule in the unit cell is shown in Fig. 2. This is obtained by extracting the single (111) layer from the fcc C_{60} solid with a standard orientation of the molecule, where the threefold axis is aligned with the [111] direction and the twofold axes are aligned with [100], [010], and [001] directions.[12] In Fig. 2, the z axis is parallel to the threefold axis of the [111] direction. Then, the x and y axes in Fig. 2 are in the (111) plane. For later sections, we denote six C atoms on the top hexagonal face of the C_{60} molecule by C1-C6 as shown in Fig. 2. When carrying out geometry optimizations, we fix the coordinates of the electrode atom and the center of mass of the C_{60} molecule so that the distance between the electrode and C_{60} layers is maintained.

Finally, there is another important thing in calculations of field-effect-doped systems. This is the treatment of the long-range Coulomb interaction in the calculations of the electrostatic potential and forces acting on atoms. To this end, we use the two-dimensional Ewald method, whose formulation differs from the three-dimensional method.[13,14] In the present study, we also take account of the multipole contribution up to octupoles. If we do not take account of the long-range Coulomb interaction with adequate accuracy, the strength of the uniform electric field between the electrode and C_{60} layers is not reproduced. Therefore, the two-dimensional Ewald method is necessary for quantitative calculations of field-effect-doped systems.

III. RESULTS AND DISCUSSION

A. Geometry optimization

We first carry out the geometry optimization of the C_{60} molecule in the neutral layer. Then, we obtain only two C-C

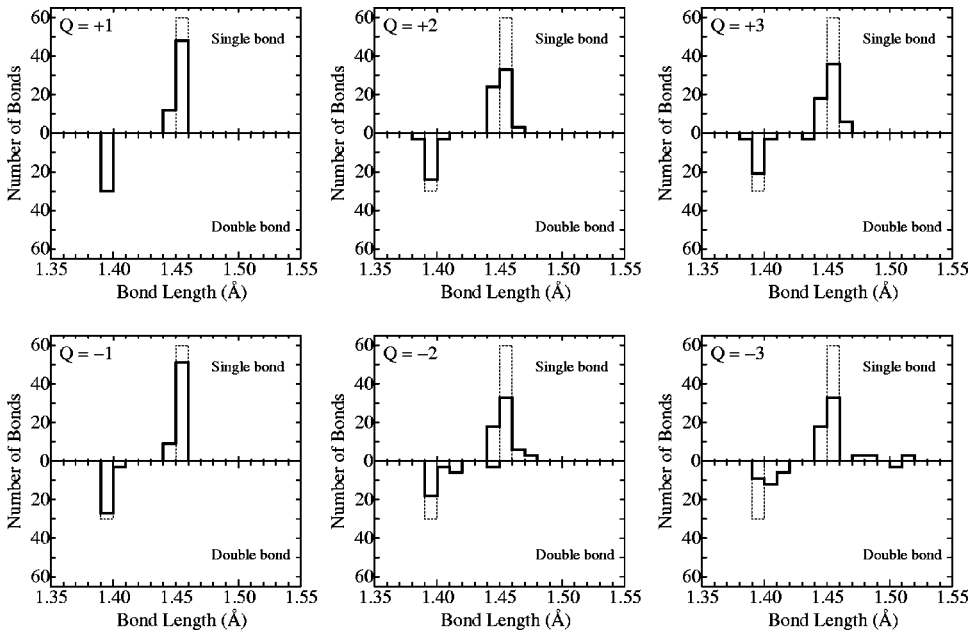

FIG. 3. Histogram for the distribution of C-C bond lengths in field-effect-doped C_{60} (solid line). The dotted line shows the distribution of C-C bond lengths in neutral C_{60}. The negative and positive Q, whose unit is e per unit cell, mean the electron and hole concentrations, respectively.

bond lengths; one is 1.45 Å which is the single C-C bond length and the other is 1.39 Å which is the double C-C bond length. These agree with the experimentally observed bond lengths of the C_{60} molecule.[15,16] That is, since the intermolecular interaction is weak, the geometry of the C_{60} molecule in the neutral layer is almost the same as the isolated C_{60} molecule.

We next carry out the geometry optimization of the C_{60} molecule in the field-effect-doped layer. Figure 3 shows the histogram for the distribution of C-C bond lengths in each carrier concentration. Here, Q denotes the carrier concentration and its unit is e per unit cell; the negative and positive Q mean the electron and hole concentrations, respectively. Although the distribution of C-C bond lengths at $|Q|=1$ resembles that in the neutral layer, there are clear changes at higher carrier concentrations. First, it is found that three double bonds are considerably elongated at $Q=-2$, -3, and $+3$. Moreover, at $Q=-3$, several single bonds are quite elongated. Thus, the deviation from the neutral geometry is increased with increasing $|Q|$. In addition, the changes from the neutral geometry are larger in electron-doped C_{60} than in hole-doped C_{60}.

The considerably elongated bonds consist of the six C atoms on the top hexagonal face shown in Fig. 2. In Fig. 4(a), we show the Q dependence of the C1-C2 double bond length, which is equal to the C3-C4 and C5-C6 double bond lengths for the threefold axis, and also show that of the C2-C3 single bond length, which is also equal to the C4-C5 and C6-C1 single bond lengths for the threefold axis. As increasing $|Q|$ both in hole- and electron-doped C_{60}, the double bond is elongated. However, at the same $|Q|$, the bond length is larger in electron-doped C_{60} than in hole-doped C_{60}. Furthermore, in electron-doped C_{60}, the single bond is elongated while this is not changed in hole-doped C_{60}. For comparison, we also show the Q dependence of the single and double bond lengths on the bottom hexagonal face in Fig. 4(b). Both single and double bonds on the bottom hexagonal face are not changed in contrast to the top hexagonal face. Also, the changes of other bond lengths except on the top hexagonal face are small.

The changes of the bond lengths in field-effect-doped C_{60} are explained by increasing and decreasing of the electron density. As we show below, the electron density on the north hemisphere of the C_{60} molecule is changed by field-effect doping while that on the south hemisphere is hardly changed. In particular, the electron density on the top hexagonal face is drastically changed. In hole-doped C_{60}, the bonding π-like electron density on the double bonds on the top hex-

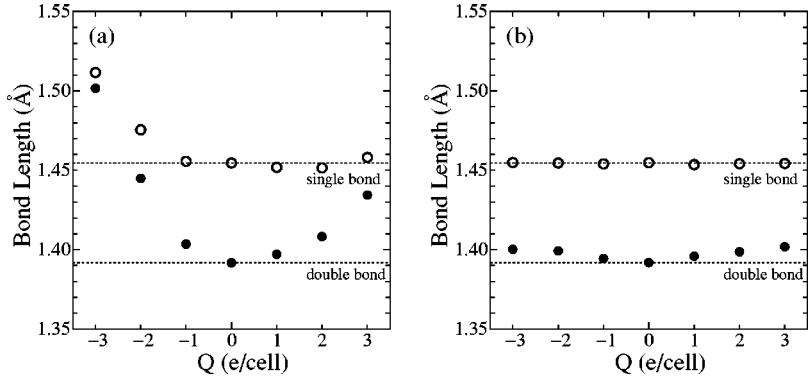

FIG. 4. The single bond length (open circles) and the double bond length (solid circles) on (a) the top hexagonal face and (b) the bottom hexagonal face. Two dashed lines show the single and double bond lengths in neutral C_{60}.

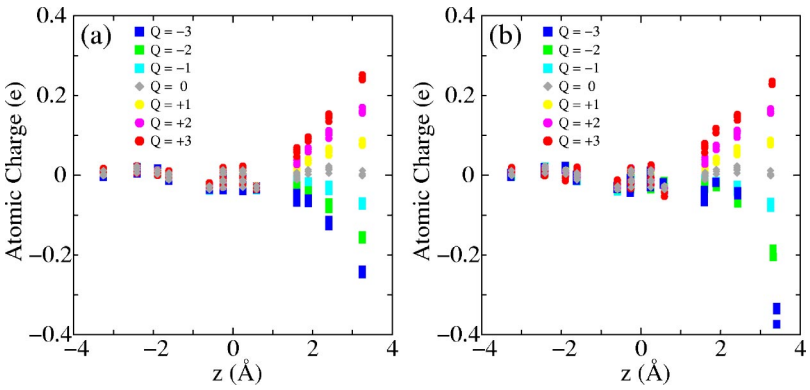

FIG. 5. Atomic charges at (a) the unoptimized geometry and (b) the optimized geometry. The horizontal axes are the z component of the position of each C atom. The z axis is set as shown in Fig. 2 and its origin is the center of mass of the C_{60} molecule.

agonal face is decreased with increasing Q. Therefore, three double bonds become weak and are elongated. In electron-doped C_{60}, since the antibonding π-like electron density on the double bonds is increased with increasing $|Q|$, these double bonds are also elongated. Furthermore, in electron-doped C_{60}, the electron density increases outside the C_{60} cage rather than inside the cage, so that the nuclei of the C atoms on the top hexagonal face are pulled outside the cage by the electron density increased outside. That is, the forces which make the whole top hexagonal face expand act on the nuclei of the C atoms. Therefore, in electron-doped C_{60}, the changes of the double bonds are larger than in hole-doped C_{60} and also the single bonds are elongated. In contrast to the top hexagonal face, the electron density on the south hemisphere is hardly changed, so that the changes of the geometry are small.

B. Charge distribution

We now discuss the charge distribution in field-effect-doped C_{60}. Figures 5(a) and 5(b) show the atomic charges at the unoptimized and optimized geometries, respectively. These are obtained by the Mulliken population analysis and represent the total charges belonging to each C atom. Here, the horizontal axes are the z component of the position of each C atom; the z axis is set as shown in Fig. 2 and also its origin is the center of mass of the C_{60} molecule.

It is found that the charge distribution is changed only on the north hemisphere of the C_{60} molecule. The qualitative results are the same in Figs. 5(a) and 5(b) although, at $Q=-3$, there are noticeably differences attributed to the large changes of the geometry. First, all C atoms in neutral C_{60} are almost neutral because the carriers are not injected. On the other hand, in hole-doped C_{60}, the C atoms on the north hemisphere ($z>0$) are positively charged. Also, those atoms are negatively charged in electron-doped C_{60}. However, the C atoms on the south hemisphere ($z<0$) are almost neutral at all the calculated carrier concentrations. That is, on the south hemisphere, the changes of the charge distribution due to field-effect doping are small.

Next, to examine the change of the charge distribution more spatially, we calculate the electron density difference $\Delta\rho(\boldsymbol{r})=\rho_f(\boldsymbol{r})-\rho_0(\boldsymbol{r})$, where $\rho_f(\boldsymbol{r})$ and $\rho_0(\boldsymbol{r})$ are the total electron densities in field-effect-doped C_{60} and neutral C_{60}, respectively; $\rho_f(\boldsymbol{r})$ is calculated at the unoptimized geometry.

We first show the result of hole-doped C_{60} of $Q=+3$. Figure 6 shows the constant electron density surface of $\Delta\rho(\boldsymbol{r})=-0.033e/\text{Å}^3$. This represents the region where the electron density is decreased by hole doping. As shown in Fig. 6, it is found that the π-like electron density on the top hexagonal face of the C_{60} molecule is decreased. It should be noted that this decreased electron density has the bonding character of double bonds.

We next show the result of electron-doped C_{60} of $Q=-3$. Figure 7 shows the constant electron density surface of $\Delta\rho(\boldsymbol{r})=0.025e/\text{Å}^3$. This represents the region where the electron density is increased by electron doping. It is found that the π-like electron density on the top hexagonal face is increased. This increased electron density has the antibonding character of double bonds.

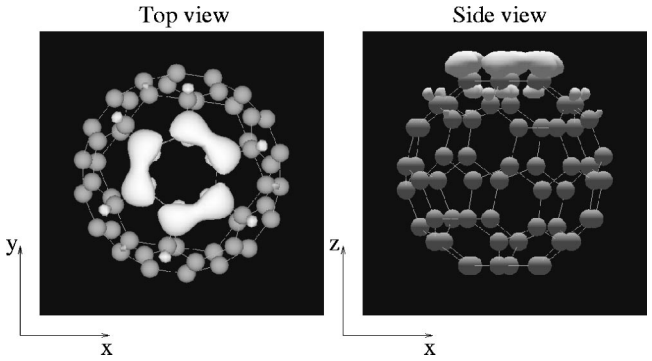

FIG. 6. Constant electron density surface of $\Delta\rho(\boldsymbol{r})=-0.033e/\text{Å}^3$ in hole-doped C_{60} of $Q=+3$.

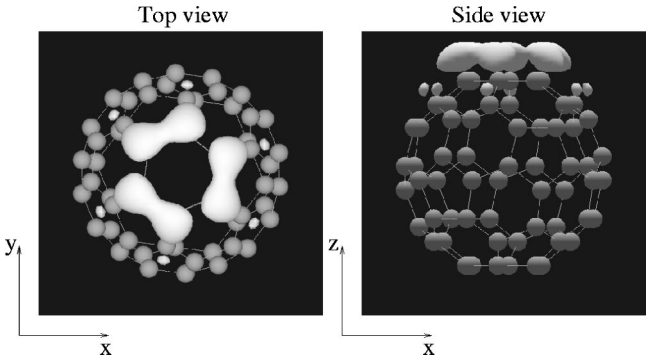

FIG. 7. Constant electron density surface of $\Delta\rho(\boldsymbol{r})=0.025e/\text{Å}^3$ in electron-doped C_{60} of $Q=-3$.

We emphasize that the changes of the electron density are consistent with the changes of the bond lengths. That is, the bonds on the top hexagonal face are elongated due to the large changes of the electron density shown in Figs. 6 and 7. In contrast, the changes of the electron density except on the top hexagonal face are not so large that the bond lengths are changed.

We here discuss the charge distribution for a more realistic system which consists of several C_{60} layers. In our single layer model, the uniform electric field generated by the electrode does not extend to the south hemisphere of the C_{60} molecule because of the screening by the charges on the north hemisphere. Furthermore, since the intermolecular interaction is week in the C_{60} solid, the interlayer interaction may be week in the real C_{60} layers. Therefore, even if we use a more realistic model which consists of several C_{60} layers, the charge distribution may be changed only on the north hemisphere in the first surface layer and the uniform electric field may not reach below the first surface layer. To confirm this, we calculate the electronic structure of the three layers of C_{60} with the (111) surface. In this three layer model, the unit cell contains three molecules and the electrode layer is 100 Å away from the first surface layer of C_{60} as shown in the inset of Fig. 8. The calculations are carried out without the geometry optimization and the Γ point in the Brillouin zone is used for the sampling of k points. Figure 8 shows the obtained atomic charges. Here, Q is the carrier concentration and its unit is e per unit cell. As expected, the C atoms in field-effect-doped C_{60} are charged only in the first surface layer while the atomic charges in the second and third layers are almost neutral. Furthermore, the atomic charges in the first layer are quite similar to those obtained in the single layer model. This means that our single layer model is valid for the calculated carrier concentrations, $1 \leqslant |Q| \leqslant 3$. In addition, we find that the carrier wave functions, which are the wave functions of the unoccupied h_u-derived bands in hole-doped C_{60} and those of the occupied t_{1u}-derived bands in electron-doped C_{60}, do not have the amplitude on the second and third layers. Thus, we conclude that the injected carriers

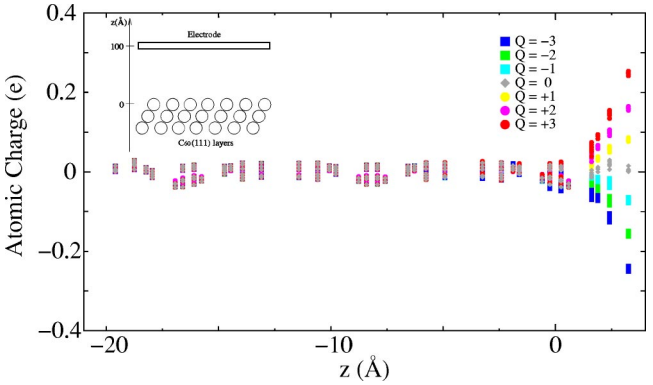

FIG. 8. Atomic charges in the three layers of C_{60} with the (111) surface. The inset is the schematic diagram of the calculated model. Q is the carrier concentration and its unit is e per unit cell which contains three molecules. The horizontal axis is the z component of the position of each C atom on the three molecules in the unit cell. The z axis is set as shown in the inset and its origin is the center of mass of the C_{60} molecule in the first surface layer.

are confined to the first surface layer for $1 \leqslant |Q| \leqslant 3$. This result is in agreement with the result obtained by a tight-binding model which consists of four layers.[17]

Moreover, it is important to compare above results with those at lower carrier concentrations because the order of $|Q|$ in the C_{60} FET's fabricated so far has been estimated to be 0.01. However, the calculations at low carrier concentrations, such as $|Q| = 0.01$, may be difficult for numerical errors. Therefore, we carry out the calculation of $Q = +0.1$ with the three layer model. In Fig. 9, we show the squared wave functions of the highest h_u-derived bands at the Γ point. For comparison, the results of $Q = 0$ and $Q = +1$ are shown together. Since the two highest h_u-derived bands are degenerate at the Γ point, we show the sum of these two squared wave functions in Fig. 9. Although the wave functions of $Q = +1$ do not have the amplitude on the second and third layers, those of $Q = +0.1$ have the noticeable amplitude on the second layer. If Q becomes lower, the wave functions

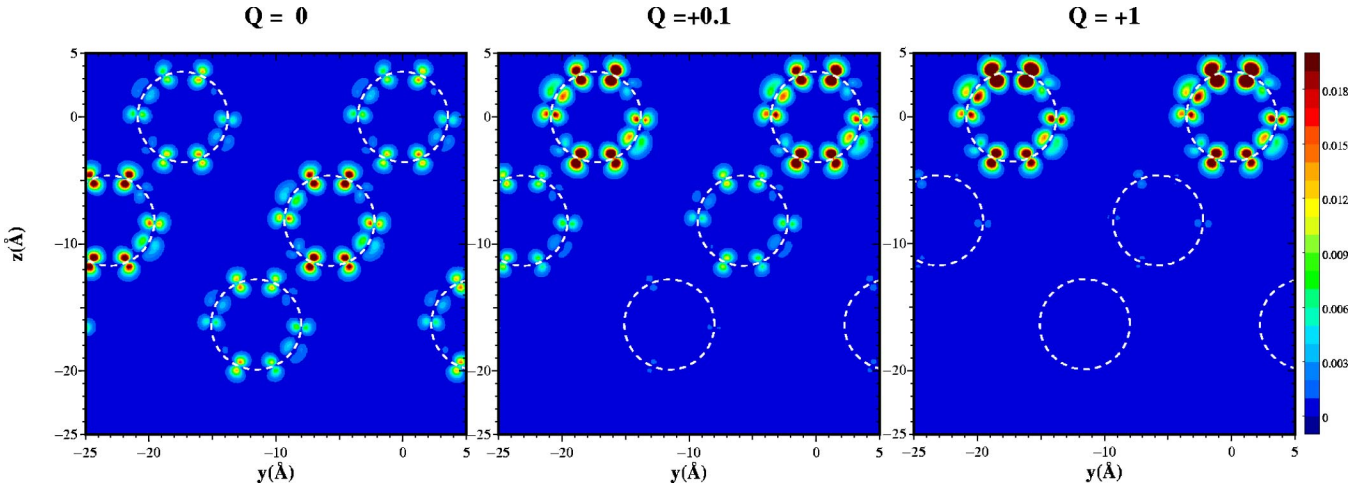

FIG. 9. Contour maps of squared wave functions of the highest h_u-derived bands at the Γ point. The white dashed lines show the spherical surfaces of the C_{60} molecules. The yz plane is corresponding to the $(\bar{1}10)$ plane of the fcc solid.

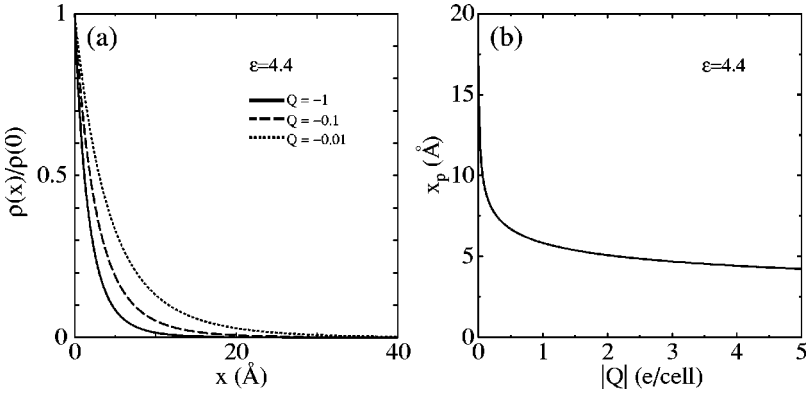

FIG. 10. (a) Electron density of the electron-doped continuum model. x is the distance from the surface of the continuum. The value of the electron density is normalized by that on the surface $\rho(0)$. (b) Penetration distance of electrons from the surface as a function of the carrier concentration Q.

may begin to resemble those of $Q=0$. This implies that, at low carrier concentrations, the carriers extend below the first surface layer.

We also calculate the charge distributions of the electron-doped continuum model by using the Thomas-Fermi method. The details of the used equations are shown in the Appendix. This calculation is not enough for the full understanding of field-effect-doped C_{60}. Nevertheless, this is useful because we can obtain the charge distributions over a wide range of carrier concentrations. In this calculation, there are two parameters. One is the dielectric constant of the neutral continuum, ε. In this paper, the used value of ε is 4.4 of the C_{60} film.[18] The other is the electron concentration per unit area, σ. However, we here represent the electron concentration by $Q=\sigma\times S$, where S is the area of the two-dimensional unit cell of the C_{60} (111) surface. In Fig. 10(a), we show the obtained electron densities at some electron concentrations. It is found that the electron density is decreased with increasing the distance from the surface, x, at any electron concentration. However, the extent of the electron distribution depends on the electron concentration. To make this clear, in Fig. 10(b), we show the penetration distance of electrons from the surface, x_p, which is defined so that 90% of the electrons exist in the region $0\leqslant x\leqslant x_p$. For $|Q|\geqslant 0.4$, x_p is smaller than the diameter of the C_{60} molecule, which is about 7 Å. This supports that the single layer model can be used for $|Q|\geqslant 0.4$. However, x_p increases with decreasing the carrier concentration; we also find that x_p is proportional to $|Q|^{-1/5}$. For $|Q|<0.01$, x_p exceeds 15 Å. This suggests that the carriers are not confined to the first surface layer in the C_{60} FET's fabricated so far.

C. Potential energy

It is worthwhile to examine how much field-effect doping affects the one-electron potential. We evaluate the potential energy of the π electron in the ath atom in the C_{60} molecule as follows:

$$V_\pi^a = \int d\boldsymbol{r}\chi_\pi^a{}^*(\boldsymbol{r})v(\boldsymbol{r})\chi_\pi^a(\boldsymbol{r}). \tag{1}$$

Here, $\chi_\pi^a(\boldsymbol{r})$ is the π orbital of the ath atom; the used π orbitals are $2p$ orbitals which are vertical to the spherical surface of the C_{60} molecule. Also, $v(\boldsymbol{r})$ is the one-electron potential, which consists of the electrostatic potential and the exchange-correlation potential. We show the calculated values of Eq. (1) of neutral C_{60} in Fig. 11(a). Furthermore, Figs. 11(b) and 11(c) show the result of hole-doped C_{60} of $Q=+3$ and that of electron-doped C_{60} of $Q=-3$, respectively. These are calculated at the unoptimized geometry. The origin of energy in Fig. 11(a) is the middle of the band gap and those in Figs. 11(b) and 11(c) are the Fermi level. The horizontal axes are the z component of the position of each C atom as well as in Fig. 5.

In neutral C_{60}, the potential energies of the π electrons are almost constant with respect to the positions of the at-

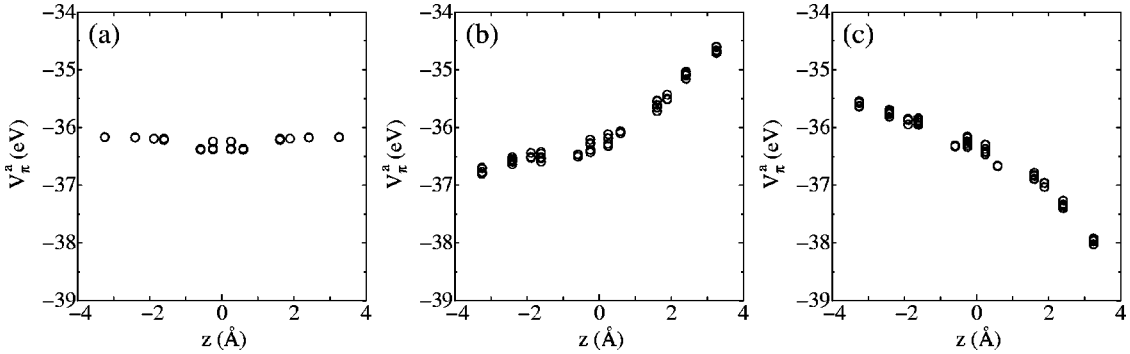

FIG. 11. The potential energies of the π electrons at (a) $Q=0$, (b) $Q=+3$, and (c) $Q=-3$. The horizontal axes are the z component of the position of each C atom. The z axis is set as shown in Fig. 2 and its origin is the center of mass of the C_{60} molecule.

oms. These results are naturally expected from the atomic charges shown in Fig. 5, where all C atoms in neutral C_{60} are almost neutral. However, the potential energies of the π electrons around $z=0$ Å are slightly lower because these π orbitals are oriented to nearest-neighbor C_{60} molecules.

In contrast, the potential energies of the π electrons in hole-doped C_{60} strongly depend on the positions of the atoms as shown in Fig. 11(b). First, the potential energies of the π electrons increase as z increases. This is due to the uniform electric field generated by the electrode. However, since the uniform electric field is screened by the charges on the C_{60} layer, the changes of the potential energy are much smaller than those expected only from the uniform electric field. In particular, the slope of the potential energy of the π electron on the south hemisphere of the C_{60} molecule is quite small because of the screening by the charges on the north hemisphere.

The potential energies of π electrons in electron-doped C_{60} shown in Fig. 11(c) are also explained as follows. In electron-doped C_{60}, the sign of uniform electric field is opposite to that of hole-doped C_{60}. Therefore, the potential energies of the π electrons decrease as z increases. Since the uniform electric field is screened as well as in hole-doped C_{60}, the changes of the potential energy are much smaller than those expected only from the uniform electric field and also the slope of the potential energy on the south hemisphere is small.

The changes of the potential energy are large enough to affect the electronic structures. As shown in Figs. 11(b) and 11(c), the potential-energy difference between at the top hexagonal face and at the bottom hexagonal face is about 2.3 eV. This difference is about 1.7 eV at $|Q|=2$ and about 1.0 eV at $|Q|=1$ although we do not show here. These differences are larger than the widths of the valence and conduction bands of neutral C_{60}. Therefore, even at $|Q|=1$, it is expected that the electronic structure alters from that of neutral C_{60}.

D. Band structure

We first show the band structure of the neutral C_{60} layer in Fig. 12. Here, the origin of energy is the middle of the band gap. The band structure of the neutral C_{60} layer is associated with the energy levels of the molecular orbitals as well as the fcc C_{60} solid.[19] The valence and conduction bands are derived from the fivefold degenerate highest-occupied molecular orbitals, the h_u orbitals, and the threefold degenerate lowest-unoccupied molecular orbitals, the t_{1u} orbitals, respectively. Furthermore, nine bands around -2.3 eV are derived from the g_g and h_g molecular orbitals. In addition, three bands around 1.8 eV are derived from the t_{1g} molecular orbitals. The calculated band widths of the valence and conduction bands are about 0.4–0.5 eV and also the band gap is about 1.3 eV.

We now show the band structures of hole-doped C_{60} in Fig. 13, which are obtained at each optimized geometry. Here, the origins of energy are the Fermi level. We also calculate the band structures of hole-doped C_{60} at the unoptimized geometry. However, since those are qualitatively the same as the results shown in Fig. 13, we show only the results at the optimized geometries; the changes of the geometry slightly affect the band structures as mentioned below.

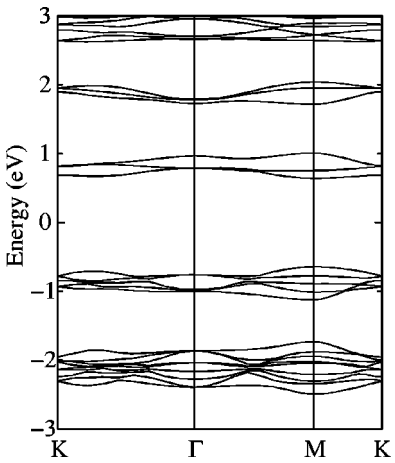

FIG. 12. The band structure of the neutral C_{60} (111) layer. The origin of energy is the middle of the band gap.

It is important to refer to the character of the wave functions. As mentioned above, the character of the wave functions in neutral C_{60} is well known. Therefore, to check those in field-effect-doped C_{60}, we calculate the square of the overlap integral, $|\langle\psi_i^{\rm n}|\psi_j^{\rm f}\rangle|^2$, where $|\psi_i^{\rm n}\rangle(|\psi_i^{\rm f}\rangle)$ is the ith eigenstate of neutral (field-effect-doped) C_{60} at the Γ point in the Brillouin zone. As a result, in hole-doped C_{60}, it is found that five bands near the Fermi level mainly consist of the h_u orbitals while there are small contributions from the g_g and h_g orbitals whose ratios are less than about 10% even at $Q=+3$. Similarly, all other bands have a main molecular orbital character and small contributions from other molecular orbitals which are energetically close to the main molecular orbitals. These results mean that the molecular orbitals are polarized in filed-effect-doped C_{60}.

Comparing the band structures of hole-doped C_{60} with that of neutral C_{60}, there are clear differences. First, in Fig. 13, the Fermi level exists into the h_u-derived bands and the system becomes metallic at all the carrier concentrations. Furthermore, the dispersion of bands is considerably different from that of neutral C_{60}. In particular, the splitting of the h_u-derived bands at the Γ point becomes larger with increasing Q. Although above results are also found at the unoptimized geometry, the splitting of the h_u-derived bands at the unoptimized geometry is smaller by up to 15% than that at the optimized geometries.

We next show the band structures of electron-doped C_{60} in Fig. 14, which are obtained at each optimized geometry. Here, the origins of energy are the Fermi level. In addition to hole-doped C_{60}, we check the character of the wave functions at the Γ point in the Brillouin zone. It is found that three bands near the Fermi level mainly consist of the t_{1u} orbitals while there are small contributions from the t_{1g} orbitals whose ratios are less than about 10% even at $Q=-3$. In all the carrier concentrations, the Fermi level exists into the t_{1u}-derived bands and the system becomes metallic. Furthermore, the dispersion of bands is considerably differ-

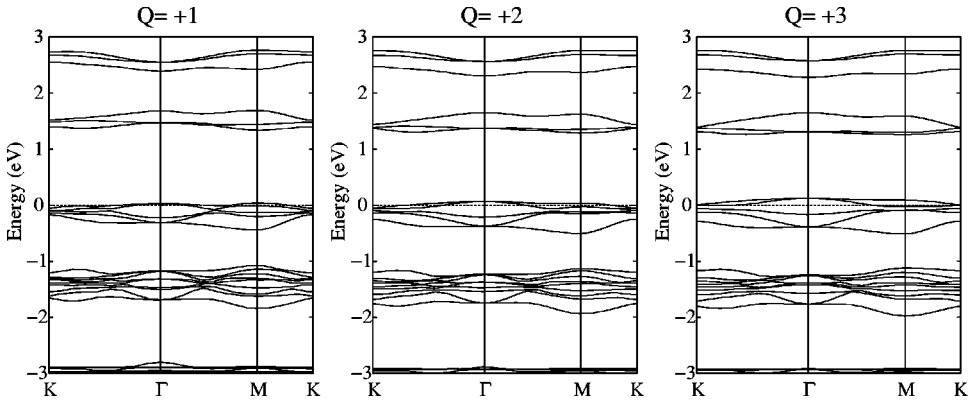

FIG. 13. The band structures of hole-doped C_{60}. The origin of energy is the Fermi level. Q is the carrier concentration and its unit is e per unit cell.

ent from that of neutral C_{60}. In particular, the splitting of the t_{1u}-derived bands at the Γ point is larger with increasing $|Q|$. The splitting at the unoptimized geometry is smaller by up to 30% than that at the optimized geometries.

E. Density of states

We finally discuss the density of states shown in Fig. 15. These are obtained at each optimized geometry. We here use Gaussian broadening with the width of 0.01 eV. Also, the origin of energy in neutral C_{60} ($Q=0$) is the middle of the band gap and those in other carrier concentrations are the Fermi level. Due to carrier doping, the Fermi level exists into the h_u-derived bands in hole-doped C_{60} and into the t_{1u}-derived bands in electron-doped C_{60}.

The features of the density of states of field-effect-doped C_{60} considerably differ from that of neutral C_{60}. These differences becomes larger with increasing $|Q|$. In particular, the density of states of the t_{1u}-derived bands is completely separated into two parts at $Q=-2$ and $Q=-3$. Also, at $Q=+2$ and $Q=+3$, the energetically lowest peak of the h_u-derived bands is considerably separated from the other peaks. These are corresponding to the level splitting at the Γ point on the band structures shown in Figs. 13 and 14. Thus, the feature of the density of states depends on the carrier concentration.

Similar results have been obtained by another theoretical study where the effects of the polarizability and the Stark splitting of the neutral C_{60} molecule are considered.[20] However, this calculation does not completely take into account effects of additional charges. Moreover, the changes of the geometry are neglected. Therefore, splitting widths of the density of states are slightly different from our results.

IV. CONCLUSIONS

In summary, we have investigated the geometry and electronic structure of field-effect-doped C_{60} by carrying out first-principles calculations based on the density-functional theory. In this paper, to reproduce field-effect doping, we have used a structural model which consists of a single C_{60} (111) layer and an electrode layer. Also, we have assumed the high carrier concentration $|Q|\geqslant 1$ in this model. We have found that the charge distribution is considerably changed only on the north hemisphere of the C_{60} molecule due to field-effect doping while the change of the charge distribution on the south hemisphere is quite small. In particular, on the top hexagonal face, the π-like electron density is decreased in hole-doped C_{60} and increased in electron-doped C_{60}. Therefore, the C-C bonds on this face are elongated with increasing the carrier concentration. Since the potential energy induced by field-effect doping is large enough to affect the electronic structures, the characters of wave functions are slightly modulated and the band dispersion is changed from that of neutral C_{60}. Moreover, reflecting such changes, the splitting of the features of the density of states appears. In the present study, we also calculate the electronic structure of the three layers of C_{60} with the (111) surface. As a result, it is found that the injected carriers are confined to the first surface layer and our single layer model is valid for the calculated carrier concentrations $|Q|\geqslant 1$. However, at a low concentration, $Q=+0.1$, we find that the carrier wave

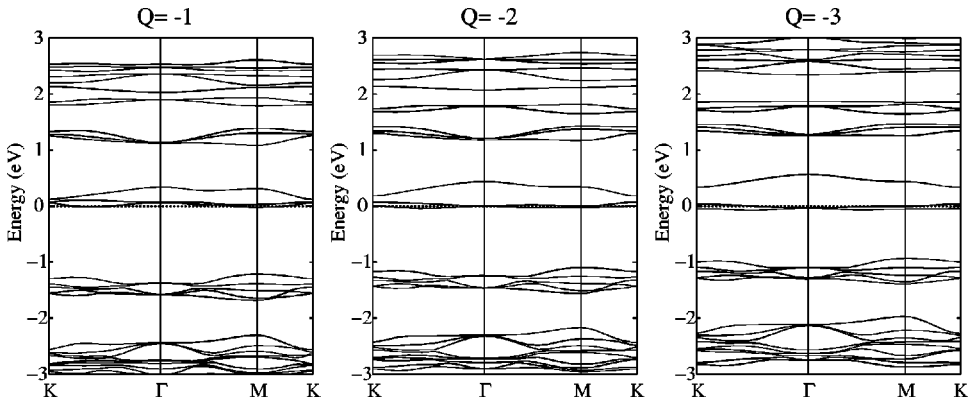

FIG. 14. The band structures of electron-doped C_{60}. The origin of energy is the Fermi level. Q is the carrier concentration and its unit is e per unit cell.

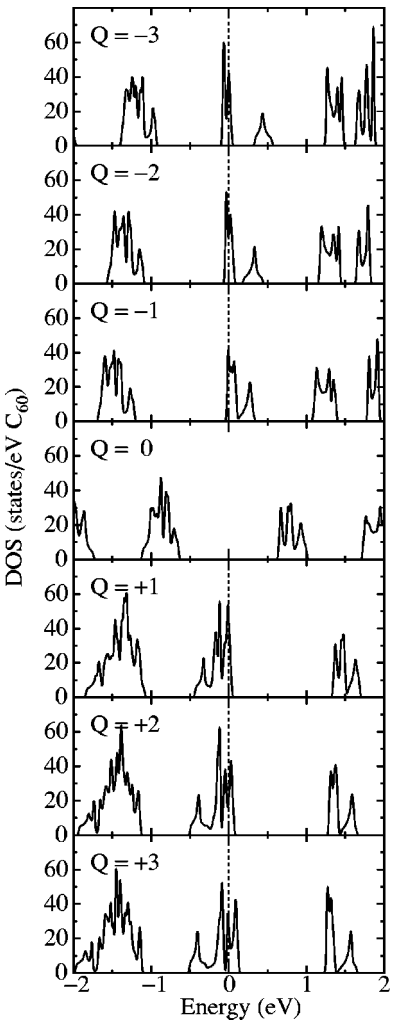

FIG. 15. The densities of states of field-effect-doped C_{60}. The origin of energy in neutral C_{60} ($Q=0$) is the middle of the band gap and those in other carrier concentrations are the Fermi level.

functions extend below the first surface layer. Furthermore, the results of the calculations with the Thomas-Fermi method show that the penetration distance of carriers from the surface is increased with decreasing the carrier concentration. Therefore, we suggest that the carriers are not confined to the first surface layer at low concentrations as obtained in the C_{60} FET's fabricated so far.

ACKNOWLEDGMENTS

This work was supported in part by the Grant-in-Aid for Scientific Research by the Ministry of Education, Culture, Sports, Science and Technology of Japan. T.C. acknowledges the support of Japan Society for the Promotion of Science. The numerical calculations were carried out on Fujitsu VPP5000 of Science Information Processing Center, University of Tsukuba.

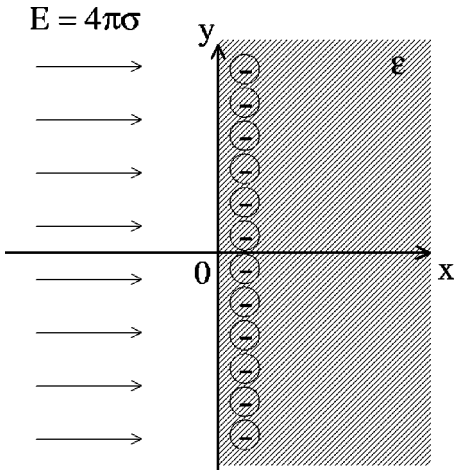

FIG. 16. Electron-doped continuum model.

APPENDIX: THOMAS-FERMI EQUATION OF THE ELECTRON-DOPED CONTINUUM MODEL

We here consider field-effect doping for the continuum. The considered circumstance is schematically shown in Fig. 16. The continuum with a dielectric constant ε lies in the half space on the positive side of the yz plane ($x>0$). The electrons are doped near the surface of this continuum (the yz plane) and its concentration per unit area is denoted by σ. Also, in the half space on $x<0$, there is the uniform electric field $E=4\pi\sigma$. In this circumstance, the Thomas-Fermi equation is given by

$$\frac{d^2\phi(x)}{dx^2}=\frac{8\sqrt{2}}{3\pi\varepsilon}\phi(x)^{3/2}, \tag{A1}$$

where $\phi(x)$ is the electrostatic potential. Also, the electron density is given by

$$\rho(x)=\frac{2\sqrt{2}}{3\pi^2}\phi(x)^{3/2}. \tag{A2}$$

To obtain the electron density, we numerically solve Eq. (A1) under the following boundary conditions:

$$\left.\frac{d\phi(x)}{dx}\right|_{x=0}=-\frac{4\pi}{\varepsilon}\sigma \tag{A3}$$

and

$$\lim_{x\to\infty}\phi(x)=0. \tag{A4}$$

Here, the first condition is derived from the continuity of the electric flux density at $x=0$. We finally check that the obtained electron density satisfies the relation

$$\sigma=\int_0^\infty dx\rho(x). \tag{A5}$$

[1] A.F. Hebard, M.J. Rosseinsky, R.C. Haddon, D.W. Murphy, S.H. Glarum, T.T.M. Palstra, A.P. Ramirez, and A.R. Kortan, Nature (London) **350**, 600 (1991).
[2] K. Tanigaki, T.W. Ebbesen, S. Saito, J. Mizuki, J.S. Tsai, Y. Kubo, and S. Kuroshima, Nature (London) **352**, 222 (1991).
[3] M.J. Rosseinsky, D.W. Murphy, R.M. Fleming, and O. Zhou, Nature (London) **364**, 425 (1993).
[4] Q. Zhu, D.E. Cox, J.E. Fischer, K. Kinaz, A.R. McGhie, and O. Zhou, Nature (London) **355**, 712 (1992).
[5] A.M. Panich, H.M. Vieth, P.K. Ummat, and W.R. Datars, Physica B **327**, 102 (2003).
[6] R.C. Haddon, A.S. Perel, R.C. Morris, T.T.M. Palstra, A.F. Hebard, and R.M. Fleming, Appl. Phys. Lett. **67**, 121 (1995).
[7] S. Suzuki and K. Nakao, J. Phys. Soc. Jpn. **66**, 3881 (1997).
[8] P. Hohenberg and W. Kohn, Phys. Rev. **136**, B864 (1964).
[9] W. Kohn and L.J. Sham, Phys. Rev. **140**, A1133 (1965).
[10] J.P. Perdew and A. Zunger, Phys. Rev. B **23**, 5048 (1981).
[11] D.M. Ceperley and B.J. Alder, Phys. Rev. Lett. **45**, 566 (1980).
[12] M.S. Dresselhaus, G. Dresselhaus, and P.C. Eklund, *Science of Fullerenes and Carbon Nanotubes* (Academic Press, San Diego, 1996).
[13] D.E. Parry, Surf. Sci. **49**, 433 (1975).
[14] F.E. Harris, Int. J. Quantum Chem. **68**, 385 (1998).
[15] C.S. Yannoni, P.P. Bernier, D.S. Bethune, G. Meijer, and J.R. Salem, J. Am. Chem. Soc. **113**, 3190 (1991).
[16] K. Hedberg, L. Hedberg, D.S. Bethuen, C.A. Brown, H.C. Dorn, R.D. Johnson, and M. de Vries, Science **254**, 410 (1991).
[17] S. Wehrli, D. Poilblanc, and T.M. Rice, Eur. Phys. J. B **23**, 345 (2001).
[18] A.F. Hebard, R.C. Haddon, R.M. Fleming, and A.R. Kortan, Appl. Phys. Lett. **59**, 2109 (1991).
[19] S. Saito and A. Oshiyama, Phys. Rev. Lett. **66**, 2637 (1991).
[20] S. Wehrli, E. Koch, and M. Sigrist, Phys. Rev. B **68**, 115412 (2003).